Contrib Mineral Petrol (2004) 147: 722–739
DOI 10.1007/s00410-004-0584-0

ORIGINAL PAPER

Valentin R. Troll · Colin H. Donaldson
C. Henry. Emeleus

Pre-eruptive magma mixing in ash-flow deposits of the Tertiary Rum Igneous Centre, Scotland

Received: 26 November 2003 / Accepted: 20 April 2004 / Published online: 13 July 2004

Abstract The Northern Marginal Zone of the Rum Igneous Centre is a remnant of an early caldera and its infill. It is composed of intra-caldera breccias and various small-volume pyroclastic deposits, overlain by prominent rhyodacite ash-flow sheets of up to 100 m thickness. The ash-flows were fed from a feeder system near the caldera ring-fault, and intrusive rhyodacite can locally be seen grading into extrusive deposits. A variety of features suggest that the ash-flows were erupted from a magma chamber that contemporaneously hosted felsic and mafic magmas: (i) chilled basaltic inclusions in rhyodacite; (ii) formerly glassy basaltic to andesitic enclaves with fluid-fluid relationships; (iii) feldspars with thick reaction rims enclosed in the basaltic to andesitic inclusions, yet with cores chemically resembling those of the rhyodacite: (iv) trace element compositions of the rhyodacite and the mafic enclaves form a mixing line between the end-member rhyodacite and basalt compositions. Additionally, textural and chemical features in the rhyodacite feldspar phenocrysts are consistent with magma mixing; (v) feldspars with resorption embayments cutting through internal zonation of the crystals; (vi) complexly zoned crystals with sieve-textured zones that are overgrown with euhedral zones; (vii) oscillatory zonation of feldspar phenocrysts in the rhyodacite, showing sharp increases in anorthite ($\Delta An \geq 10\%$) followed by gradual decrease in An-content ($\Delta An \leq 4\%$). This evidence points to eruption of ash-flows from a felsic magma chamber that was periodically replenished by injection of mafic magma. Diffusional mixing between the two magmas was permitted by temperature and compositional differences, but was slow due to the contrast in viscosities and densities. The Fe–Ti–P-enriched basic magma that replenished the chamber was degassing on entering the lower temperature environment and soon equilibrated thermally, followed by chemical exchange between the two end-member magmas. This process formed hybrid andesite enclaves enriched in trace elements beyond that caused by simple mixing, implying trace element diffusion in addition to bulk mixing. Eruption was caused by replenishment with, and degassing of, the basic magma and the chamber partially evacuated while the process of hybridisation was underway. The erupted products record magma mixing by chamber replenishment, blending of two magmas and elemental exchange in the magma chamber, and also physical mingling in the eruptive conduit.

V. R. Troll (✉)
Department of Geology, Trinity College, College Green,
Dublin 2, Ireland
E-mail: trollv@tcd.ie

C. H. Donaldson
School of Geosciences, University of St Andrews,
The Irvine Building, St Andrews,
KY 16 9AL, Scotland

C. H. Emeleus
Department of Earth Sciences, University of Durham,
South Road, Durham, DH1 3LE, England

Introduction

Many intimate associations of felsic and mafic rocks are reported from major and minor composite intrusions in the British Tertiary Igneous Province (BTIP) (e.g. Harker 1904; Blake et al. 1965; Walker and Skelhorn 1966; Elwell et al. 1974; 1974; Gamble 1979; Thompson 1980; Bell 1983; Sparks 1988; Bell and Emeleus 1988; Kerr et al. 1999). The case has been made that such composite intrusions provide not only compelling evidence of the operation of compositional zonation and magma replenishment in chambers but also an opportunity to observe coexisting magmas frozen during violent emplacement (e.g. Marshall and Sparks 1984). Two generic models can explain such occurrences of intimate association of felsic and mafic rocks: (a) protracted fractional crystallisation modified by mixing and replenishments (cf. Marshall and Sparks 1984), and (b) replenishment of a magma chamber by input of a con-

trasting magma type that more or less mixes with the resident magma to produce hybrids (Eichelberger et al. 2000). The key difference between the models is that in the former the mafic to felsic rock compositions represent a co-genetic suite modified by magma mixing, whereas in the latter the magmas coexisted in a common reservoir but were derived from distinct sources, being thus co-eruptive but not co-genetic.

A mixed rhyodacite–andesite–basalt suite occurs in feeder dykes, plugs and associated ash-flow deposits of the Northern Marginal Zone of the Rum Igneous Centre. Basaltic chilled margins on a composite feeder dyke and enclaves in intrusive and extrusive rhyodacite ash-flow deposits are taken to represent mafic magma that coexisted with felsic magma compositions. This felsic–mafic suite offers a link between magma chamber processes, dyke intrusion and surface volcanism. It also provides an opportunity to compare the mixing behaviour of contrasting magmas in a common magma reservoir, in feeder conduits above the reservoir and within the resulting ash-flow deposits themselves. Using field, petrographic and chemical evidence, we distinguish between physical mixing of rhyodacite and basalt on eruption (mingling) and pre-eruptive chemical magma mixing (hybridisation) in order to assess the genetic relationship between the mafic and the felsic magma compositions. We also document previously unreported field observations and new geochemical data on this classical example of a mixed-magma occurrence, one of the few remnants of explosive silicic volcanism in the BTIP, and suggest that the mafic magma replenished a felsic magma chamber and initiated a complex mixing process that ended in the ash-flow eruptions.

Geological setting and previous work

The rocks preserved in the Northern Marginal Zone of the Rum Centre have been described and interpreted previously (including Judd 1874; Geikie 1888; Harker 1908; Bailey 1945; Dunham 1965, 1968; Emeleus 1997; Troll et al. 2000) and are only briefly summarised here.

The caldera basement is formed by uplifted Lewisian gneisses (Archaean) and Torridonian sediments (Precambrian), overlain by an intra-caldera collapse breccia succession with minor interbedded pyroclastic units up to 170 m thick (Emeleus 1997). The breccias are succeeded by 3–6 m of epiclastic sandstone that is overlain by thick (> 100 m) rhyodacite ash-flow sheets (Emeleus 1997). The rhyodacites of the Northern Marginal Zone (historically called 'felsites' in the BTIP) have been a matter of debate for more than 100 years (compare Emeleus 1997; Donaldson et al. 2001) and only recently have they been clearly identified as intra-caldera ash-flow deposits (Williams 1985; Bell and Emeleus 1988; Emeleus 1997; Troll et al. 2000). Emeleus (1997) further determined that the Rum rhyodacites are intra-caldera ash-flows that had risen through feeder dykes before spreading on an intra-caldera topography of caldera-collapse breccias.

The age of formation of the Northern Marginal Zone (i.e. the rhyodacite) predates the formation of the Rum Layered Suite of peridotites, troctolites, anorthosites, and gabbros (60.5 ± 0.1 Ma, Hamilton et al. 1998). While general aspects of the petrology and mineralogy of the rhyodacites have been published (cf. Hughes 1960; Dunham 1965, 1968; Emeleus et al. 1971; Emeleus 1997), no comprehensive petrological and geochemical account is yet available and the mafic enclaves have previously not been examined in detail.

Analytical techniques

XRF Central pieces of samples were sectioned by rock saw and selected for whole-rock analyses, avoiding cracks and rims affected by alteration. Samples for whole-rock analyses were crushed and powdered in agate ball-mills. Samples were dried at 110°C prior to analysis. Major and trace elements were determined by XRF on fused beads using a Philips PW1212 spectrometer at the University of St Andrews and an automated Philips PW1480 spectrometer at GEOMAR Research Centre, Kiel, Germany. All analyses were performed with a Rh tube; calibration was performed using international geological reference samples. Several samples were analysed on both machines and very similar results have been obtained.

EMP Samples were prepared as polished thin sections for optical microscopy and electron microprobe analyses. Mineral and glass analyses were performed on a JEOL 733 Superprobe at the University of St Andrews, using wavelength-dispersive spectrometry. Analytical conditions included an acceleration voltage of 15 kV, a beam current of 8–20 nA, and counting times of between 20 and 60 s on peaks. A rastered beam was used for feldspar (ca. 12 μm^2), and for glass (ca. 40 μm^2). Natural and synthetic minerals were used as standards and monitors.

ICPMS Trace elements and REE were analysed by Inductively Coupled Plasma-Mass Spectrometry on a Perkin Elmer Sciex ELAN 5000 at Actlabs Ancaster, Canada. Analytical procedure and uncertainties are available at: http://www.actlabs.com.

TIMS Sr and Pb isotopic ratios of the two end-member rock compositions were measured at GEOMAR Research Centre, Kiel, on a Finnigan MAT 262 thermal ionisation mass spectrometer (TIMS) in a static mode. Prior to dissolution, all samples were leached for 1 h in HCl at 120°C. Chemical separation techniques have been described in Hoernle et al. (1991). Replicate analyses were within analytical uncertainty. $^{87}Sr/^{86}Sr$ was fractionation-corrected within-run to $^{86}Sr/^{88}Sr$ of 0.1194 and the precision of the standard runs for NBS987 was

0.710254 ± 11. Replicate analyses yielded an external reproducibility better than 0.000015. The Pb isotope data on these samples (Table 4), including analytical procedure and conditions, are available in Geldmacher et al. (2002).

The Rum rhyodacites

Field relations

The rhyodacites compose the upper units of the pyroclastic succession that infill the early Rum caldera (Troll et al. 2000). The succession is summarised in Fig. 1.

Three main masses of rhyodacite are distinguished in the Northern Marginal Zone: the Western Mass (Am Màm), the Central Mass (Meall Breac) and the Eastern Mass (Cnapan Breaca) (Fig. 1.). The northern part of the Western Mass has steep to vertical, intrusive contacts with the intra-caldera mesobreccias (max. clast size · 1 m; Lipman 1976) and earlier intrusive rocks, forming a system of rhyodacite feeder dykes. Traced southwards it passes into an extrusive sheet, up to 40 m in thickness and dipping at ~25–30° to the south. The sheet was deposited onto a palaeo-topography of valleys and ridges (compare Dunham 1968; Emeleus 1997). The Central Mass too has a steep-sided intrusive contact in the north passing southwards into an extrusive sheet that dips ~25–30°S. At its southern limit the sheet is approximately 100 m thick and can be seen to infill a palaeo-valley within the mesobreccia. The Eastern Mass comprises three parts: a tabular sheet of approximately 80 m in thickness to the south that forms the hill Cnapan Breaca, a pipe-like plug north of Cnapan Breaca up to 150 m wide, and near the Main Ring Fault several narrow dykes orientated parallel to the ring-fault (dykes not shown in Fig. 1).

Stratigraphic correlation and petrologic features indicate that the three major rhyodacite masses are part of same rock body (Troll et al. 2000). While the individual rhyodacite masses were each mapped as a single unit, interbedded lithic tuff horizons and rhyodacite-free breccia layers on Meall Breac and Cnapan Breaca indicate that the Eastern and the Central Masses include the products of at least three major eruptions or eruptive pulses ('major flow units', Fig. 1.). The rhyodacite eruptions were accompanied by caldera collapse, as recorded in the interbedded breccia horizons within the extrusive rhyodacite at, for example grid location [NM 395 975] (Fig. 1.) and in post-depositional downfaulting of the extrusive rhyodacite at, for example, the southern end of Meall Breac at [NM 385 983].

In outcrop and in thin section, the rhyodacite is characterised by eutaxitic textures (fiamme) (Fig. 2) defining a sub-horizontal, and in places a rheomorphically folded, foliation. Jointing perpendicular to the foliation is observed locally. Fiamme are of two types: a light-grey type that is poor in phenocrysts (< 10%) and a darker grey type that is relatively phenocryst-rich (> 20%). The crystal-poor fiamme are largely confined to the lower parts of the first major flow unit (Fig. 1). The eutaxitic texture is abundant in the lower two major flow units and becomes progressively less prominent upwards, probably reflecting the decrease in load pressure up-section. There is an increasing abundance of mafic and mixed inclusions in the upper parts of each major flow unit (Fig. 1), as well as a general increase in mafic components up-section through the rhyodacite flow units.

The steeply dipping feeder dykes to the rhyodacite sheets occur in all three rhyodacite masses, all in the northernmost part of the Northern Marginal Zone. They cut through the intrusive Am Màm Breccia and the sedimentary Coire Dubh Breccias, showing a variance of dip directions ranging from ~60° to the south to vertical to ~60° to the north. Pronounced foliation within the dykes, picked out by highly attenuated fiamme, is generally parallel to the smooth, planar margins. This fracture geometry picked out by the dykes resembles that of fault systems ascribed to magmatic over-pressure in a doming or resurgence stress field (see Troll et al. 2000 and references therein).

Rhyodacite petrography

Stratigraphically below the rhyodacite are thin crystal and lithic tuffs in the Coire Dubh breccias (Fig. 1). These tuffs form layers up to 20 cm in thickness, traceable over about 100 m. The lithic tuffs contain various accidental "pick-up clasts" of lithologies that make up the caldera-infill breccias and abundant angular to blocky glass shards of mafic through felsic compositions. The crystal tuffs contain abundant plagioclase feldspar and subordinate alkali-feldspar plus quartz and minor clinopyroxene. Mafic schlieren and basalt fragments are present.

The main rhyodacite lithologies (intrusive and extrusive) contain phenocrysts of plagioclase (~10–30 vol%), quartz (< 5 vol%), minor pyroxene (~3 vol%) and accessory opaque oxides. Biotite and hornblende occur as alteration products around the pyroxene phenocrysts. The groundmass varies in character from microcrystalline quartz + alkali feldspar + hornblende + iron oxide, to cryptocrystalline with fine banding and flattened, now devitrified, glass shards.

Quartz phenocrysts are up to 3 mm in size. Many have a square outline, indicative of ß-quartz cut parallel or nearly parallel to the c-axis and most display rounded corners and embayments (Fig. 3a,b). The pyroxene phenocrysts were described in detail by Emeleus et al. (1971) who emphasised that complex zoning in many of the crystals records disequilibrium between crystals and the melt.

Plagioclase phenocrysts show varying sizes from < 0.02 mm to > 4 mm. Crystal size generally increases towards the top of the extrusive succession. The plagioclase morphologies vary from broken and embayed to euhedral crystals and many show internal zonation

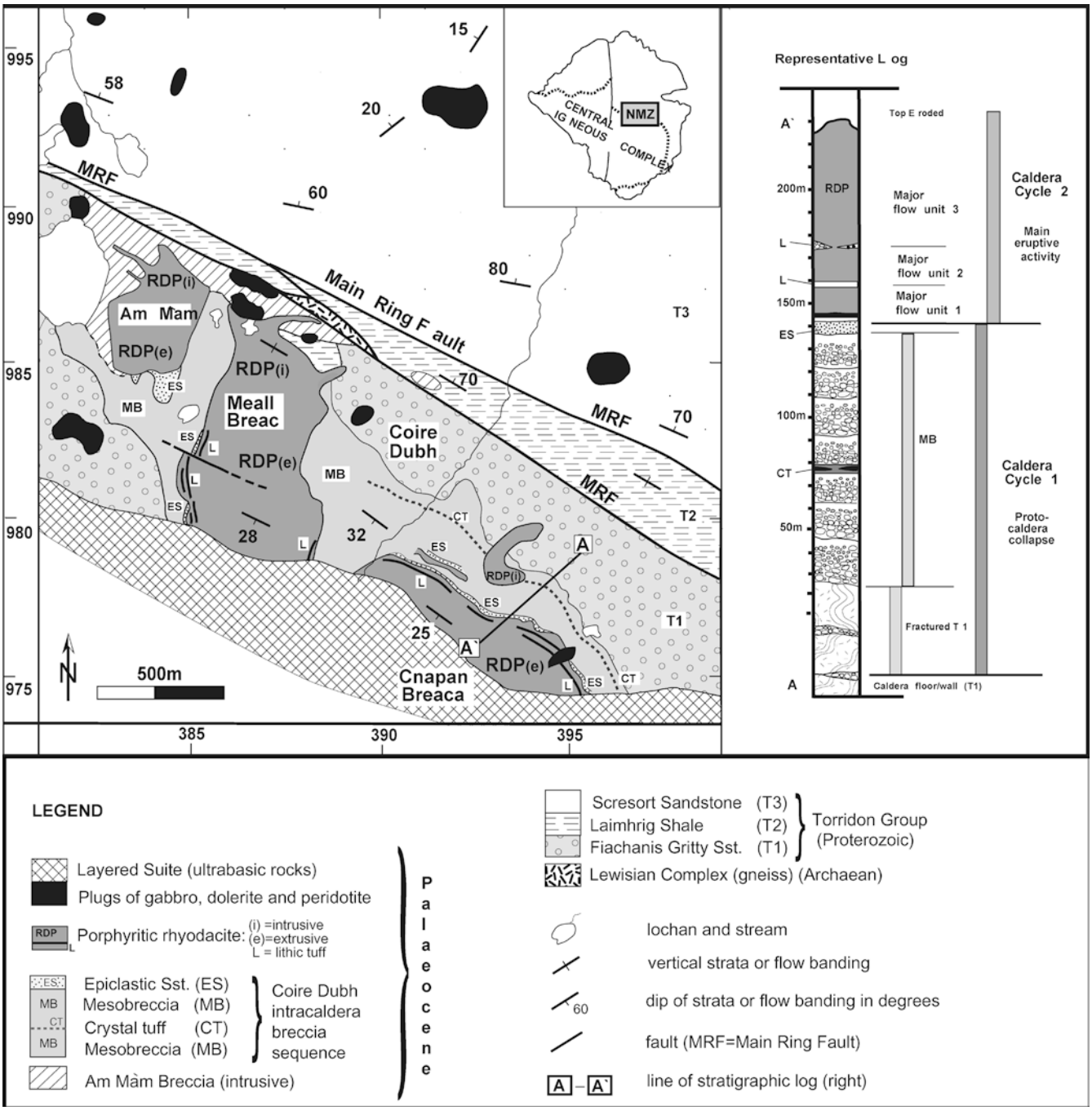

Fig. 1 Map of the Northern Marginal Zone (*left*) and stratigraphic log section through the intra-caldera succession (*right*), modified from Troll et al. (2000). Coordinates refer to British Grid Reference System (*NGRS*)

(Fig. 3; Table 1). The compositional range is $An_{16–34}$ and there is oscillatory zoning (Fig. 4). All twelve crystals analysed show one or more sharp increase(s) in anorthite content followed by a gradual decrease in successive zones. Up to four zones are present within individual crystals and the anorthite content of a zone typically rises sharply outwards by up to $\Delta An \geq 10$ mol%, but decreases by just $\Delta An \leq 3–4$ mol% in the following zones.

There are no phenocrysts of alkali feldspar in the rhyodacite, in contrast to the early crystal tuffs. In addition, the early tuffs contain plagioclases that have a slightly more evolved compositional range ($An_{15–27}$).

Mafic inclusions in the rhyodacite

Mafic inclusions are scarce in the early crystal tuffs but much more abundant in the rhyodacite ash-flow deposits. Three main types were identified by Troll et al. (2000), of which type II and type III are discussed here in great detail:

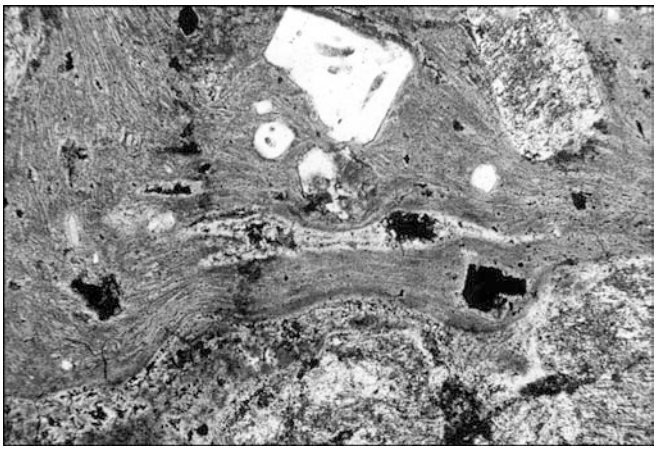

Fig. 2 Photomicrograph of compacted pumice in rhyodacite. Field of view ca. 4 mm, PPL. Broken crystal above fiamme is quartz

Type I inclusions are coarse-grained plutonic xenoliths of chiefly gabbroic compositions. They are rare and occur throughout the deposits. These are considered to be accidental fragments from the walls of the magma chamber and/or the eruption conduit.

Type II inclusions are dark, aphyric, cryptocrystalline basalts and andesites. These inclusions occur as blobs, streaks, schlieren and fragments and are found in discrete horizons, up to 1.5 m thick in the rhyodacite deposits and are concentrated at the margins of some of the intrusive feeder plugs and dykes. Emulsion textures, absence of chilled exteriors, and inferred fluid-fluid relationships (wavy junctions) have been observed between type II enclaves and the rhyodacite host, implying that blobs of mafic magma and the rhyodacite magma had a sufficiently small temperature difference for chilling not to occur. These inclusions were interpreted as a liquid magma that co-existed with the rhyodacite host.

On the east side of Meall Breac, at [NM 387 984], a several metres thick composite sheet that grades along strike into extrusive rhyodacite, comprises a chilled mafic margin and a rhyodacite interior with abundant type II inclusions (Fig. 5a). The chilled margin has the most primitive rock composition found in the suite of samples (sample CDCM-1-1 in Table 2) and is virtually aphyric. The fluid–fluid relationship of the inclusions against the rhyodacite host offers a possible explanation for the existence of type II inclusions in the extrusive rhyodacite ash-flow deposits. Entrainment of one magma in the other during ascent of the two magmas in the conduit appears to be very similar to the entrainment features observed in experimental simulations of the two-phase conduit flow (e.g. Freundt and Tait 1986).

The plug that forms part of the Eastern Mass of rhyodacite [NM 393 980] has an irregular contact with the country rock and consists of a co-mingled rhyodacite host and up to 50% basic inclusions of type II. The inclusions range from finely dispersed emulsion textures to cm-sized blobs (Fig. 5.), and are most abundant in the marginal zones of the plug. In the absence of an extrusive equivalent, the plug is assumed to have been the pipe feeder of a late rhyodacite eruption that would have been markedly enriched in mafic inclusions.

Type III inclusions are also basaltic, are always round and have a microcrystalline texture with plagioclase lath morphologies characteristic of quenching (cf. Lofgren 1980). The inclusions show a pronounced chilled margin (Fig. 6a–c). This type is also found throughout the rhyodacite rather than being confined to certain stratigraphic horizons. Troll et al. (2000) considered these to represent chilled magma clots that solidified on contact with the rhyodacite host magma during chamber replenishment. The majority of these inclusions are vesicle-free and only about 10–15% have gas bubbles.

Geochemistry

Major and trace elements

Representative samples of extrusive rhyodacite, rhyodacite feeder dykes, co-mingled rocks, type II and type III inclusions, and the chilled mafic margin of the Meall Breac composite sheet were analysed for major and trace elements (Table 2).

The major oxide characteristics of the rhyodacite and the co-existing mafic compositions indicate that two distinct end-member magmas were involved, each with a well-defined compositional range (Fig. 7a). The rhyodacite analyses form a tight compositional cluster, whereas the mafic compositions range from 50–60 SiO_2 wt% and from 5–3 wt% MgO, with type II inclusions showing the highest SiO_2 and lowest MgO concentrations.

Trace element co-variation diagrams also show that the mafic compositions plot along a mixing line in element vs. element and ratio vs. ratio plots and along a mixing curve in element ratio vs. element ppm plots (Fig. 7b). Ratios with Sr and Y show that the correlation is independent of the effects of variable plagioclase and ferromagnesian mineral abundance in the samples. The rhyodacite samples too show a spread in all trace element plots, defining their own mixing lines and curves.

REE and isotopes

On a chondrite-normalised REE variation diagram, the patterns for a representative rhyodacite and the most primitive chilled dyke margin basalt (type III composition) crosscut each other, with the rhyodacite being enriched in LREE and the basalt in HREE (Table 3; Fig. 8a). This crosscutting relationship indicates that the two magmas are genetically distinct and unlikely to originate by some simple parent–daughter relationship such as fractional crystallisation of the coexisting mafic magma (cf. Bell 1983). Moreover, the rhyodacite has no appreciable negative Eu anomaly as would be expected

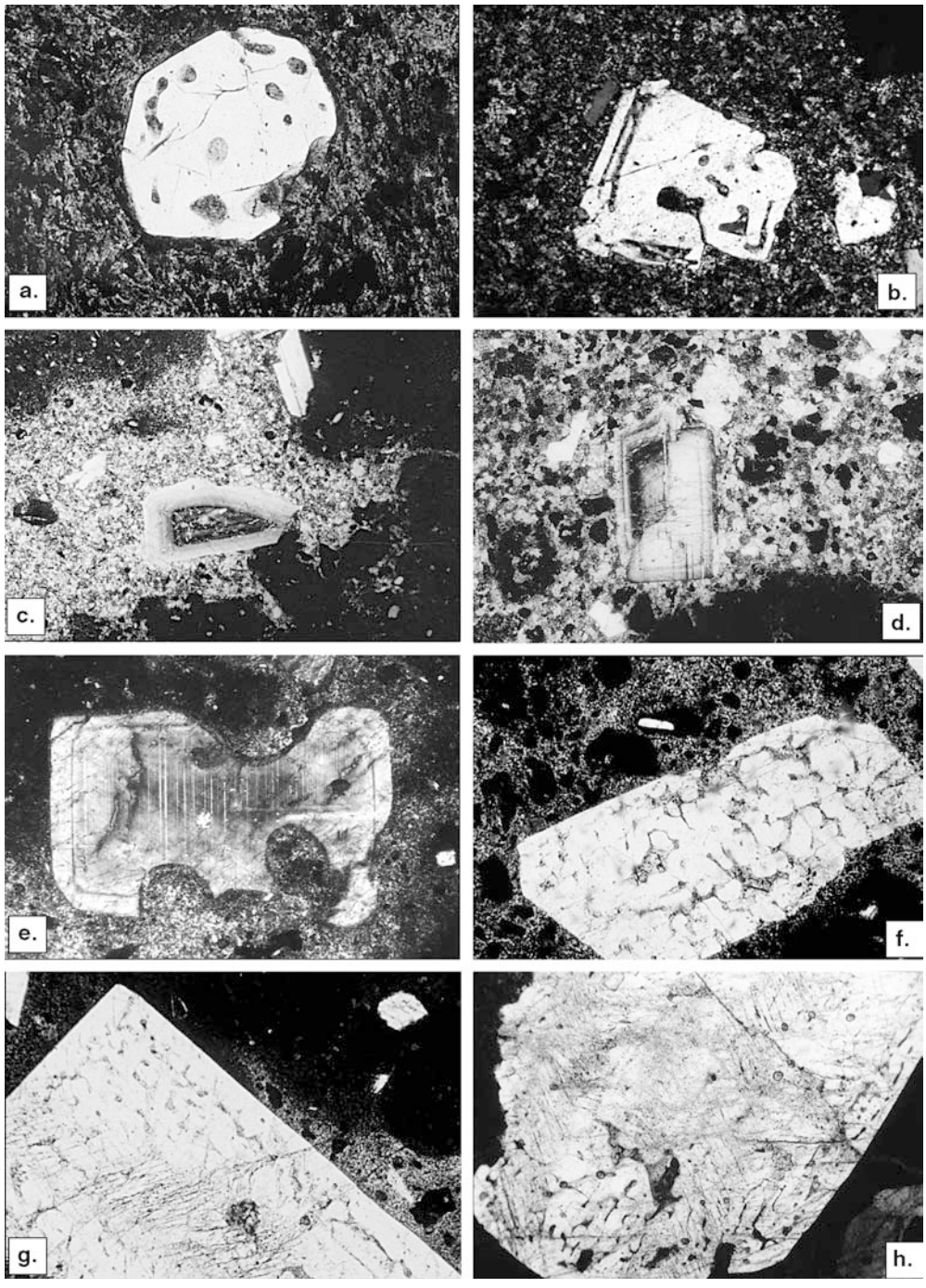

Fig. 3 Photomicrographs of (**a, b**) embayed quartz crystals in rhyodacite, Field of view ca. 2 mm, PPL. (**c, d**) Zoned plagioclase crystals in rhyodacite, Field of view ca. 3 mm, CPL. (**e**) Resorbed plagioclase crystal in rhyodacite plug N-Cnapan Breaca (note embayments cut across internal zoning), field of view ca. 2 mm, CPL. (**f**) Sieve texture plagioclase associated with mafic magma inclusions, rhyodacite plug N-Cnapan Breaca, Field of view ca. 2 mm, PPL. (**g**) Sieve texture zone in plagioclase with euhedral overgrowth, rhyodacite plug N-Cnapan Breaca. Field of view ca. 1.5 mm, PPL. (**h**) Resorbed plagioclase crystal with internal sieve texture zone, rhyodacite plug N-Cnapan Breaca. Field of view ca. 1.5 mm, PPL

in the case of an origin through prolonged fractionation of plagioclase (cf. Civetta et al. 1998; Freundt and Schmincke 1995), the most abundant phenocryst of the rhyodacite. Separated plagioclase from the rhyodacite shows a marked positive Eu anomaly (Fig. 8b). One possibility for the lack of a negative Eu anomaly in the rhyodacite may be the input of an Eu-rich component (contaminant?) that counteracted Eu removal through plagioclase fractionation, thus preventing a substantial negative-Eu anomaly from forming (cf. Troll and Schmincke 2002).

The basalt is marked by LREE enrichment and displays a slightly positive Eu anomaly. This is either the result of (a) some LREE input from the rhyodacites or (b) interaction with country-rock, or (c) the basalt is derived from an enriched source.

The two most primitive basalt samples (chilled dyke margin of type III composition), two representative rhyodacite samples, and a rhyodacite plagioclase separate were also analysed for Sr and Pb isotopes (Table 4) to constrain the origin and evolution of the two end-member compositions. The data (corrected to 60 Ma)

Table 1 Representative plagioclase analyses

	Plagioclase No. 12/29										Plagioclase No. 35/11										Plagioclase No. 28/34										Plagioclase No. 05-36									
Sample	Pos 1	Pos 3	Pos 5	Pos 6	Pos 7	Pos 8	Pos 9	Pos 10	Pos 1	Pos 2	Pos 3	Pos 5	Pos7	Pos 8	Pos 2	Pos 3	Pos 4	Pos 5	Pos 7	Pos 8	Pos 9	Pos 1	Pos 3	Pos 5	Pos 7	Pos 8	Pos 9	Pos 10
SiO_2	63.54	60.77	62.68	63.84	62.99	62.58	61.42	63.14	63.97	63.64	62.21	62.63	63.78	63.68	63.47	61.67	62.36	63.43	61.12	62.08	61.14	62.26	60.71	60.62	61.46	61.30	61.46	61.89
Al_2O_3	22.68	24.02	22.71	22.15	22.92	22.78	23.45	22.92	22.78	22.73	23.56	23.82	22.63	22.46	22.49	23.47	23.48	23.08	23.81	23.51	24.04	22.21	23.98	23.97	22.92	21.53	22.62	22.27
FeO	0.31	0.26	0.28	0.28	0.24	0.26	0.34	0.36	0.29	0.30	0.33	0.31	0.14	0.31	0.23	0.23	0.33	0.22	0.19	0.20	0.28	0.31	0.25	0.32	0.36	0.24	0.36	0.33
CaO	3.79	5.62	4.07	3.35	4.04	4.25	5.03	4.02	3.88	3.94	5.07	4.91	3.82	3.44	3.91	4.98	4.77	3.99	5.26	4.66	5.57	3.43	5.81	6.22	4.70	3.13	4.89	4.04
Na_2O	9.26	8.01	9.28	8.32	9.39	9.56	8.90	9.43	9.38	9.15	8.49	9.17	9.92	9.68	9.62	8.82	9.23	9.62	8.93	9.27	9.04	8.30	7.96	7.90	8.26	3.32	8.13	9.10
K_2O	0.80	0.59	0.62	1.20	0.41	0.23	0.42	0.35	0.60	1.06	0.95	0.42	0.18	0.49	0.41	0.42	0.19	0.12	0.26	0.29	0.25	1.69	0.66	0.23	0.80	8.69	1.08	0.63
Total	100.38	99.27	99.64	99.14	99.98	99.66	99.57	100.23	100.90	100.82	100.61	101.26	100.47	100.06	100.13	99.57	100.36	100.44	99.57	100.01	100.31	98.19	99.37	99.26	98.49	98.21	98.55	98.26
O	3.012	2.969	2.998	2.987	2.987	3.002	2.967	2.977	3.031	3.021	3.006	3.030	3.021	3.008	3.007	2.982	3.007	3.021	2.978	2.997	2.994	2.943	2.969	2.968	2.951	2.879	2.946	2.946
Si	2.809	2.725	2.772	2.794	2.845	2.794	2.726	2.747	2.811	2.805	2.756	2.752	2.811	2.819	2.811	2.754	2.761	2.796	2.732	2.758	2.719	2.817	2.723	2.719	2.773	2.835	2.777	2.798
Al	1.181	1.270	1.210	1.193	1.163	1.198	1.259	1.236	1.180	1.181	1.230	1.234	1.175	1.172	1.174	1.235	1.225	1.199	1.254	1.231	1.260	1.184	1.268	1.267	1.219	1.174	1.205	1.186
Fe	0.011	0.010	0.010	0.010	0.010	0.009	0.015	0.013	0.011	0.011	0.012	0.011	0.005	0.011	0.009	0.008	0.012	0.008	0.007	0.007	0.010	0.012	0.009	0.012	0.014	0.009	0.014	0.013
Ca	0.180	0.270	0.225	0.194	0.160	0.192	0.271	0.241	0.183	0.186	0.241	0.231	0.180	0.163	0.185	0.238	0.226	0.188	0.252	0.222	0.265	0.166	0.279	0.299	0.227	0.155	0.237	0.196
Na	0.794	0.696	0.759	0.801	0.719	0.807	0.725	0.772	0.799	0.782	0.729	0.781	0.848	0.831	0.825	0.763	0.793	0.822	0.774	0.798	0.779	0.728	0.692	0.687	0.722	0.298	0.713	0.797
K	0.045	0.034	0.053	0.035	0.068	0.023	0.023	0.024	0.034	0.060	0.054	0.023	0.010	0.028	0.023	0.024	0.011	0.006	0.015	0.016	0.014	0.098	0.038	0.013	0.046	0.513	0.062	0.036
Total	5.020	5.005	5.029	5.028	4.966	5.022	5.019	5.033	5.016	5.025	5.021	5.033	5.030	5.024	5.027	5.022	5.028	5.019	5.035	5.034	5.048	5.004	5.009	4.997	5.001	4.983	5.008	5.026
An	18.45	27.94	22.86	19.51	18.20	19.21	27.20	23.79	18.61	19.22	24.81	22.83	17.55	16.41	18.33	23.81	22.20	18.63	24.56	21.74	25.39	18.57	28.75	30.30	23.92	34.25	24.95	19.70

Pos Positions correspond to Fig. 4

show that the rhyodacite is strongly enriched in radiogenic Sr and displaced towards the composition of the local upper continental crust (Lewisian amphibolite) on a Sr vs. Pb plot and on a Pb vs. Pb plot (Fig. 9a,b). The rhyodacite appears to contain a substantial crustal component (see also Geldmacher et al. 2002). These results are in accord with the Sr isotope data obtained from the Western granite by Meighan (in Emeleus 1997). In contrast, the basalt samples of the chilled dyke margin have isotope ratios that are substantially less radiogenic and plot well within the mantle array for Tertiary Hebridean mantle (e.g. Dickin 1981; Ellam and Stuart 2000). The basalt samples are therefore considered to have experienced limited interaction with crustal components during ascent.

Discussion

Field evidence

The intra-caldera ash-flows of the Rum Centre exhibit all features of classical ignimbrites, including compaction and welding, eutaxitic textures, various depositional pulses, as well as plugs and steeply dipping feeder dykes that pass into extrusive deposits. The feeder dykes are roughly parallel to the Main Ring Fault and pass into the extrusive sheets in the case of the Western and the Central rhyodacite masses (cf. Troll et al. 2000). These outcrop relationships are considered characteristic of intra-caldera settings (e.g. Almond 1971; Walker 1984). Almond reported very similar vertical and steeply dipping feeder dykes to extrusive ignimbrites from the Sabaloka caldera and ascribed them to the opening of tensional fractures above a resurgent dome subsequently dilated by rising acidic magma. Likewise Walker (1984) ascribed silicic vent rings within and outside the ring-fault of calderas as likely to represent 'cone sheet fractures' caused by magmatic over-pressure.

Plagioclase textures and compositional zoning

Plagioclase zoning is often interpreted as recording the history the host magma has experienced (e.g. Pearce and Kolisnik 1990; Stamatelopoulou-Seymour et al. 1990; Tepley et al. 1999). In the rhyodacite, several types of zoning are present, some with an overall increase in An from core to rim and some with an overall decrease. All crystals analysed, however, show one or more sharp increase(s) in anorthite content followed by a gradual decrease in successive zones (Fig. 4). Such sharp increases of ~10 mol% An that are associated with internal resorbtion surfaces (Fig. 3), followed by more or less gradual decreases in An content over successive zones, are commonly associated with magma mixing (e.g. Nixon and Pearce 1987; Pearce and Kolisnik 1990; van Wagoner et al. 1995; Tepley et al. 1999).

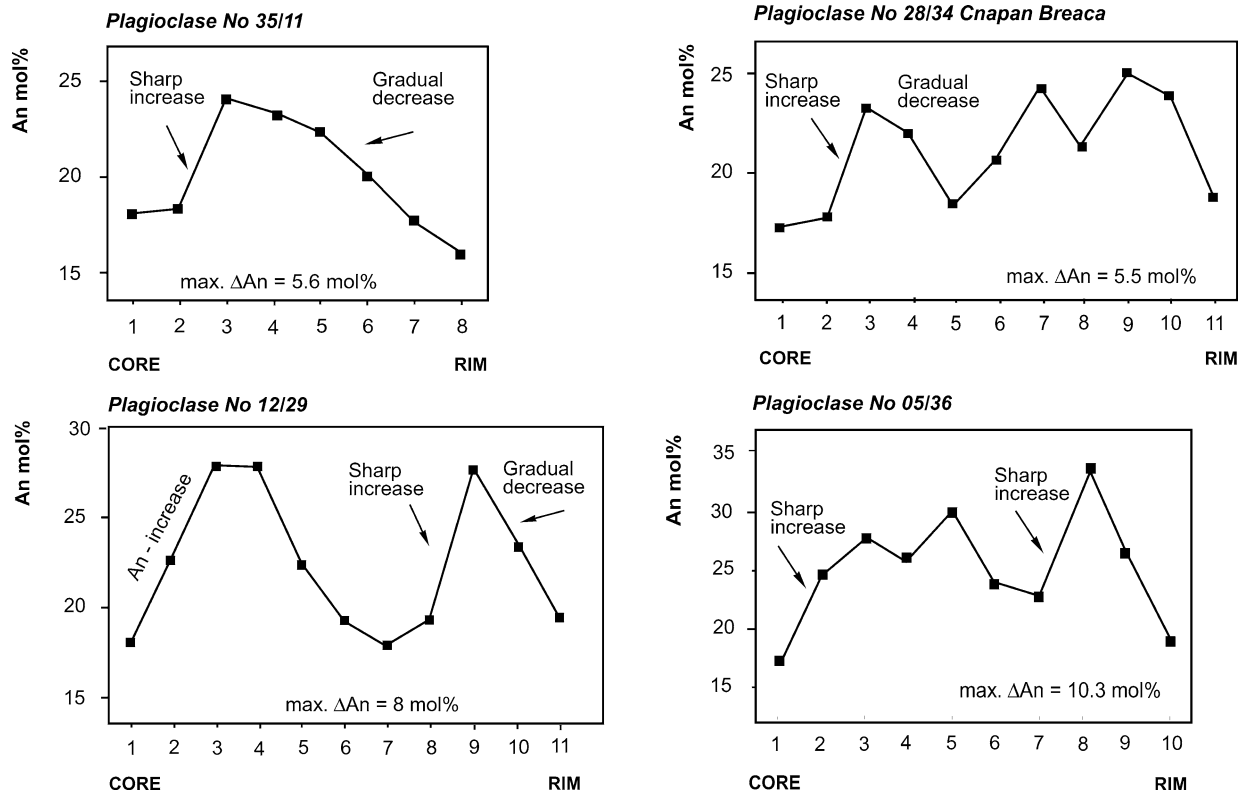

Fig. 4 Representative core to rim profiles of plagioclase phenocrysts. Distance between measured points is 0.2 mm for all points. See text for details

We interpret these zoning patterns in the rhyodacite plagioclases as representing a combination of (a) fairly stable growth of crystals from a progressively evolving melt, resulting in gradual decreases in An content, and (b) periodic inputs of heat and changes to more mafic melt composition resulting in initial resorption (Fig. 3-e,f) and then in anorthite-enriched overgrowth (Fig. 3g). If the most complexly zoned plagioclase crystals are interpreted this way, then three to four major events of magma replenishment occurred. The plagioclase zoning is consistent with the embayed textures in other minerals in the rhyodacite, including pyroxene (see Emeleus et al. 1971) and quartz (see Fig. 3a,b), pointing to multiple magma chamber replenishments by more mafic magma during the lifetime of the rhyodacite magmatic system.

Mechanism(s) of magma mixing

The mafic inclusions and the rhyodacite represent two distinct magmas that co-existed in the same magma chamber, as evidenced by type II inclusions that lack quench textures (chilling) and display fluid–fluid relationships with the host rhyodacite. Another line of evidence is the strongly resorbed plagioclase crystals of the rhyodacite enclosed in the type II enclaves (Fig. 5), supporting co-existence of the two magmas in the chamber for sufficient time to allow crystal transfer between magmas and the development of thick reaction rims. The evidence from inclusions in the rhyodacite plug suggests that thermal equilibrium between batches of the two magmas was closely approached. However, it needs to be stressed that the emulsion textures in samples from the rhyodacite plug and from the early interbedded tuffs, represent the final process of mixing in the magma chamber as well as physical mixing in the exit conduits. In the conduit, entrainment of one in the other was forced upon the two co-existing magmas by eruption and associated caldera collapse. We infer that the type II inclusion magma must have been adjacent to the rhyodacite for considerable time prior to the eruption, allowing for both thermal and chemical interaction between the end-member magmas.

In marked contrast, type III inclusions were clearly in thermal dis-equilibrium with the rhyodacite host. From morphology and texture it appears that the type III inclusions were virtually solid at the time of eruption, whereas the rhyodacite host was largely liquid, a criterion used by Sparks and Marshall (1986) to suggest large initial temperature contrast between the felsic host magma and the inclusion magma. Therefore type III inclusions must have formed prior to physical mixing in the conduit. They are thought to have formed in the magma chamber. Their round shape and chilled margins imply that chilling was rapid, and so there was no time for their deformation in the highly viscous felsic host (cf. Sparks et al. 1977; Eichelberger 1980). This is also supported by the absence of vesicles in the majority of the type III mafic inclusions, suggesting that rapid quenching prevented vesiculation.

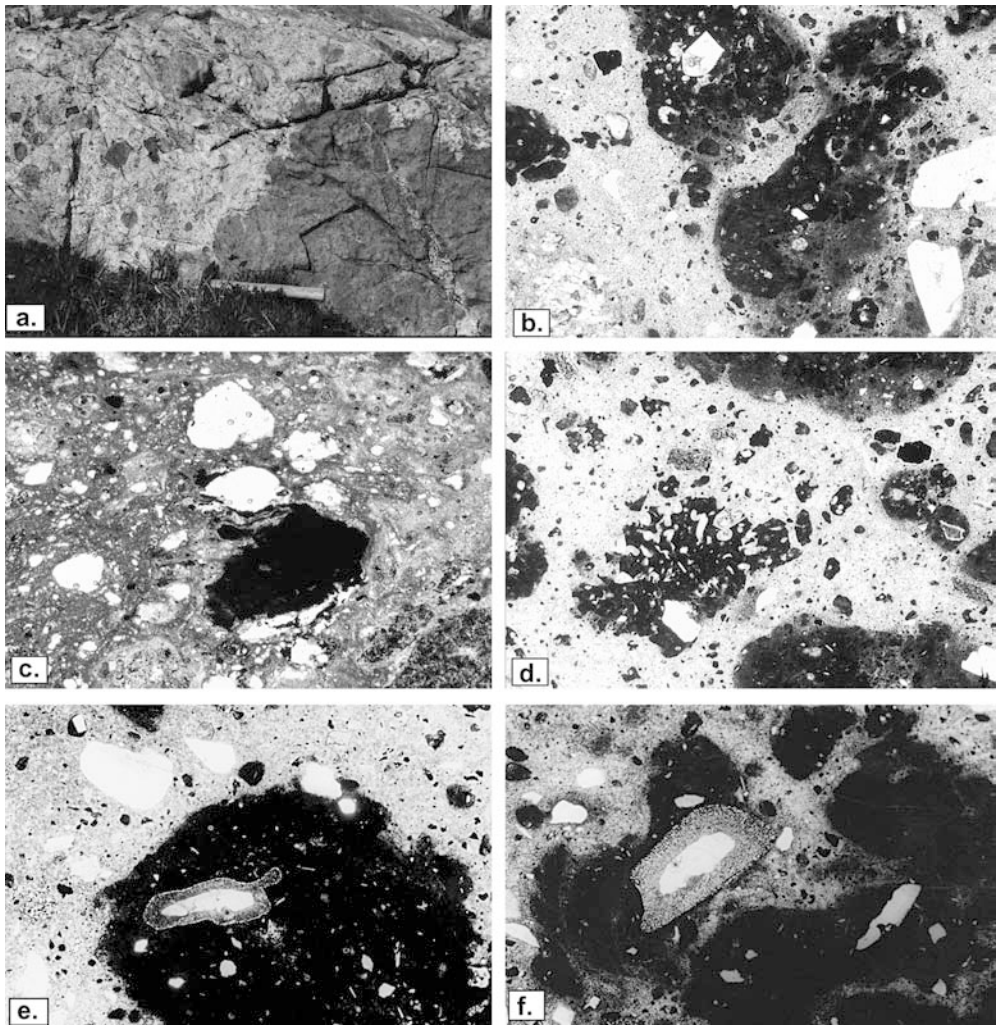

Fig. 5 **a** Mafic pillow in composite rhyodacite feeder dyke at north end of Meall Breac. Note hammer for scale. **b** Photomicrograph of emulsion texture formed by interaction of mafic type II inclusions with rhyodacite host in the plug north-west of Cnapan Breaca (Fig. 1). Field of view ca. 5 mm, PPL. **c** Photomicrograph of plastically deformed type II inclusion in feeder dyke North of Meall Breac. Field of view ca. 5 mm, PPL. **d** Formerly glassy basaltic to andesitic inclusions, with plastically deformed vesicles and sharp edges suggesting quenching during fragmentation by decompressional degassing (Cnapan Breaca plug. Field of view ca. 3 mm, PPL). **e, f** Rhyodacite-derived plagioclase crystals in type II inclusions (*centre*) showing resorbed corners and a broad reaction-rim against the basalt/andesite host inclusion. Note other plagioclase crystal in contact with both basalt and rhyodacite. Field of view ca. 5 mm, PPL

Coombs et al. (2002) recently distinguished two major types of crystalline mafic inclusions (termed enclaves in their paper) in eruptive felsic rocks. Their 'type 1 enclaves' closely resemble Rum type III inclusions, and are proposed to form during mafic replenishment of a felsic magma chamber. Thereby, the mafic magma breaks up into discrete lumps or pillows upon entering the felsic chamber, forming inclusions within the felsic host, either by convective motion in the host magma or by forceful injection into it. As the inclusions lose heat to the felsic host they crystallise inwards, leading to a gradation from small crystals at the exterior to larger crystals in the more slowly cooled interior (cf. Bacon 1986). The 'type 2 enclaves' of Coombs et al. (2002) more closely match the Rum type II inclusions. They envisaged these to arise from a mafic replenishment that forms a layer of mafic magma at the bottom of a felsic magma chamber, thereby creating a mafic–felsic interface. Heat transfers upwards across this interface and as crystallisation proceeds in the cooling mafic layer, volatile exsolution causes density inversion that allows mafic magma blobs to float into the felsic host. These 'type 2 enclaves' are characterised by a random range of crystal sizes (including the absence of crystals), reflecting crystallisation in the mafic bottom layer rather than direct interaction of the enclave with the felsic host.

We propose that the chilled Rum type III inclusions also resulted when mafic magma fountained into a felsic magma chamber. During this process, the replenishing mafic magma was engulfed in felsic magma and chilled as microgranular inclusions. Fountain replenishments have been proposed for many outcrops in the BTIP (e.g. Blake et al. 1965; Walker and Skellhorn 1966) and their dynamics have been examined in experimental studies (e.g. Campbell and Turner 1989). However, most of such a replenishing magma would have eventually collected at the base of the magma chamber due to density contrast, forming a bottom layer with a semi-stable mafic–felsic interface in-between (cf. Sparks et al. 1977; Huppert and Turner 1981; Blake and Koyaguchi 1991; Wiebe 1996; Wiebe et al. 2001). This accumulated bottom layer is, in turn, represented by the apparently thermally equilibrated type II inclusions. The compositional variation among the mafic inclusions points to a possible chemical zonation of the mafic magma, with more silicic (andesitic) melt grading downward into basaltic melt.

Table 2 Representative major and trace element concentrations Representative major and trace element analysis of rhyodacite and co-existing mafic compositions

Sample No.	Rhyodacite								Rhyodacite						Mafic inclusions and chilled dyke margins						Co-mingled andesite	
Rock type	NETLH-1 rhyodacite	NETLH-3 rhyodacite	NMBDP-1 rhyodacite	NMBDP-3 rhyodacite	SWCBDP-1 rhyodacite	SWCBDP-2 rhyodacite	STLH-1 rhyodacite	STLH-2 rhyodacite	SMBDP-4 rhyodacite	DPMB-1 rhyodacite	DPMB-2 rhyodacite	UDPN-1 rhyodacite	UDPN-2 rhyodacite	CDCM-1-1 basaltic margin	CDCM-1-2 basaltic margin	DPP-ME type 3 inclusion[a]	DPP-ME-1 type 2 inclusion	DPP-ME-2 type 2 inclusion	DPP-ME type 2 inclusion[a]	DPP-BR-1 comingled WR	DPP-BR-2 comingled WR	DPP-BR-4 comingled WR
wt%																						
SiO_2	71.75	71.34	72.09	71.82	72.2	71.65	71.37	70.60	71.40	71.62	72.53	70.86	70.96	51.7	51.55	52.09	58.61	57.48	55.49	62.46	62.66	61.75
TiO_2	0.68	0.66	0.67	0.69	0.68	0.65	0.73	0.69	0.62	0.63	0.65	0.75	0.70	2.33	2.34	2.17	1.80	1.81	2.14	1.47	1.45	1.43
Al_2O_3	12.83	12.57	12.57	12.77	12.85	12.61	13.07	12.79	12.19	12.32	12.6	13.11	12.99	13.64	13.63	13.15	13.10	13.29	13.28	13.25	13.15	12.85
Fe_2O_3	4.81	4.49	4.52	4.89	4.81	4.44	5.06	4.64	4.63	4.31	4.62	5.15	4.92	14.76	14.84	12.94	10.99	11.02	11.39	9.64	9.54	9.18
MnO	0.1	0.09	0.09	0.1	0.08	0.08	0.1	0.09	0.09	0.08	0.08	0.1	0.09	0.23	0.23	0.21	0.16	0.17	0.20	0.15	0.14	0.15
MgO	0.22	0.48	0.49	0.27	0.19	0.43	0.26	0.50	0.56	0.39	0.17	0.19	0.40	4.67	4.71	4.68	3.26	3.33	3.76	2.42	2.45	2.57
CaO	1.81	1.77	1.70	1.74	1.6	1.59	1.95	1.91	1.67	1.26	1.31	1.9	1.87	8.41	8.41	9.64	6.20	6.27	7.89	5.02	5.08	4.95
Na_2O	4.41	4.43	4.41	4.18	4.44	4.83	4.43	4.52	4.56	4.32	4.2	4.46	3.99	3.34	3.37	5.17	3.53	3.49	4.75	3.75	3.8	4.22
K_2O	3.13	3.05	3.20	3.27	3.22	3.19	3.06	3.01	3.37	3.36	3.48	3.11	3.05	0.92	0.93	0.22	1.60	1.51	1.25	2.12	2.14	2.12
P_2O_5	0.12	0.13	0.13	0.13	0.12	0.13	0.14	0.13	0.12	0.13	0.12	0.14	0.13	0.31	0.31	ND	0.24	0.26	ND	0.21	0.2	0.21
Total	99.86	99.71	100.47	99.86	100.19	100.40	100.17	100.48	99.91	99.12	99.76	99.77	100.00	100.49	100.48	100.81	100.08	99.36	100.19	100.69	100.61	99.73
LOI	0.35	0.70	0.60	0.4	0.35	0.80	0.35	1.60	0.70	0.70	0.45	0.4	0.90	0.4	0.3	ND	0.6	0.7	ND	0.5	0.5	0.30
Ppm																						
Ba	972	979	976	958	943	955	962	979	967	974	974	971	997	294	270	ND	515	526	ND	623	ND	652
Nb	12	12	12	10	12	12	11	11	11	12	14	12	12	8	8	ND	8	8	ND	12	ND	8
Ce	140	103	102	91	107	105	108	82	94	99	91	126	103	43	40	ND	65	67	ND	55	ND	72
La	24	49	47	19	29	49	31	39	45	47	19	25	52	12	14	ND	30	29	ND	13	ND	33
Y	26	27	30	29	27	28	21	21	28	30	29	29	32	34	33	ND	32	33	ND	32	ND	31
Zr	264	268	278	273	273	278	257	260	300	287	285	258	262	164	165	ND	202	199	ND	220	ND	219
Pb	15	18	15	15	16	14	12	9	13	14	13	14	14	16	24	ND	7	7	ND	15	ND	6
Rb	91	90	94	99	100	98	92	89	105	92	97	91	89	35	34	ND	48	50	ND	65	ND	63
Sr	215	208	200	204	206	200	234	226	179	169	177	245	237	299	300	ND	239	241	ND	253	ND	241
Th	4	7	7	4	8	6	6	5	7	7	3	4	7	4	4	ND	5	5	ND	8	ND	5

[a]Determined by EMP; *ND* not determined

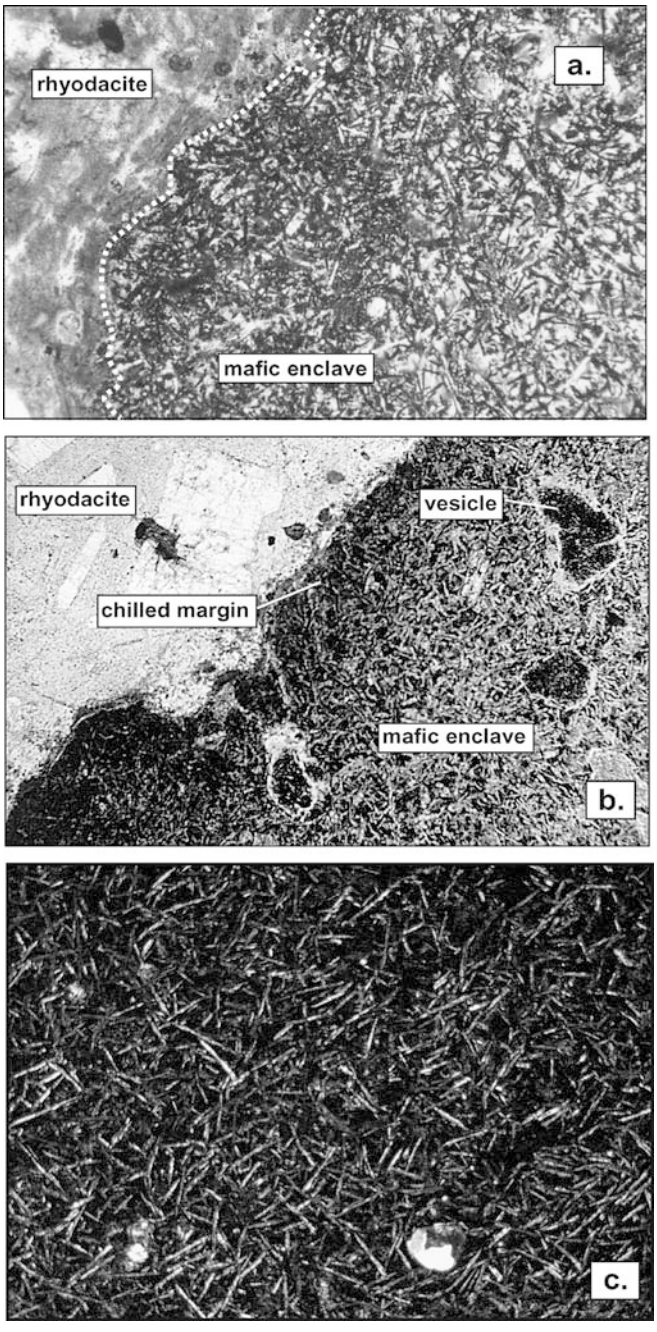

Fig. 6 **a** Photomicrographs of chilled, vesicle-free, mafic inclusion in the rhyodacite. Grain-size of the plagioclase laths decreases towards the crenulate margin, implying quenching of the inclusion. In addition, the elongate and skeletal plagioclases indicate rapid crystal growth in the inclusion's interior, consistent with enhanced under-cooling of the melt. Field of view ca 6 mm, PPL. **b** Chilled, vesicular, mafic inclusion in rhyodacite. Field of view ca. 6 mm, PPL. **c** Close up of the marginal zone of a chilled mafic enclave. Crystal size and abundance increases towards the inclusion interior (*bottom*). Field of view ca. 0.5 mm, PPL

A further process may have produced type III enclaves at this stage. At the interface between the rhyodacite host and the mafic magma, vesicles forming in the latter may have caused blobs of basalt to rise buoyantly into the felsic host. The blobs vesiculated further and chilled by undercooling and thermal contact with the much cooler rhyodacite (cf. Eichelberger 1980). This process may be recorded in the much less abundant type III enclaves that are vesiculated (Fig. 6b).

Chemistry of magma mixing

Samples of co-mingled rock from the Cnapan Breaca plug, i.e. rhyodacite with abundant type II inclusions, are andesitic in whole rock composition and represent a physical aggregate of mafic and felsic end-member components that is close to a 50:50 binary mixture (Fig. 7). They are taken to represent a bulk mixture of the mafic and the felsic magma. These co-mingled andesites consistently plot on a mixing line between the two end-members in chemical variation diagrams.

Applying simple binary mixing relations to the major oxide compositions of the mafic samples, the compositions most strongly affected by chemical mixing are type II mafic inclusions, some of which consist of a mixture of 30% of rhyodacite and 70% basalt (Fig. 10a). The rhyodacites, in turn, do not exhibit evidence for magma mixing in their major oxide compositions, but do so in their trace element concentrations. Assuming the rhyodacite to have been chemically fairly uniform prior to the mixing event(s), trace element mixing calculations show that up to 30% of its lithophile and incompatible elements (Rb, Zr, Ce) were lost to the basalt (Fig. 10b). However, this is inconsistent with simple bulk mixing of major elements and trace elements. For instance, reduction of 30% of Rb in rhyodacite by binary mixing with basalt would create a hybrid with a SiO_2 content of 65 wt%, assuming a SiO_2 concentration of 71 wt% and of 51 wt% as starting compositions for rhyodacite and basalt, respectively. In turn, modelling of compatible elements such as Sr and Y (Fig. 10c) suggests that while the rhyodacite clearly lost incompatible elements, it gained compatible elements, e.g. up to 25% of the Sr and Y in the most affected rhyodacite samples may be basalt derived (Fig. 7). This trace element exchange inferred from the rhyodacite samples is also reflected in the trace element concentrations of the hybrid type II inclusions. Whereas major oxide modelling suggests the most hybridised mafic inclusions are a mixture of ca. 70 parts basalt to 30 parts rhyodacite, trace element modelling of incompatible elements suggests a mixture of about 55 parts basalt to 45 parts rhyodacite (Fig. 10b). Modelling of compatible trace elements such as Sr (Fig. 10c) shows the hybrid inclusions to be depleted in Sr relative to their Zr content and the rhyodacites to be enriched in Sr (relative to their Zr content), a distribution pattern also observed in other mixed magma occurrences (e.g. Gamble 1979; Platevoet and Bonin 1991).

This trace element distribution requires the operation of a chemical exchange process in addition to bulk hybridisation. Since both the rhyodacite and the mafic inclusions are affected by this additional process, it must

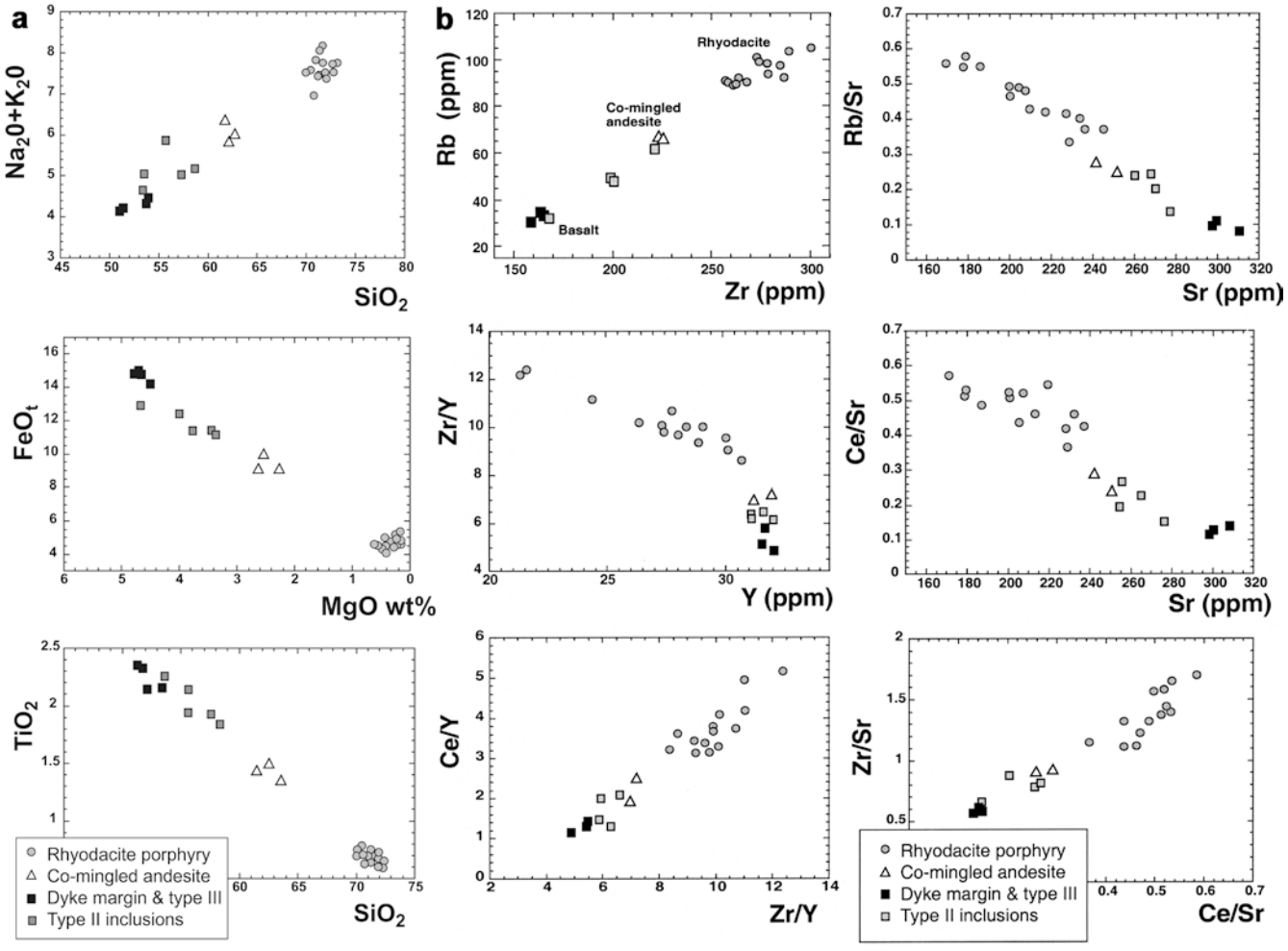

Fig. 7 **a** Major oxide variations between rhyodacite (*circles*), mafic inclusions and the chilled margin of a composite dyke (*squares*), and bulk rock analysis of co-mingled rocks (*triangles*). Unlike the mafic compositions that range from basalt to andesite, rhyodacite samples have uniform composition. **b** Linear and curved pattern of rock compositions in various trace element variation diagrams show that rhyodacite samples plot along mixing lines and curves

Table 3 REE concentrations (ppm) of rhyodacite, plagioclase and basalt

	Sample No. and type		
	UDPN 3 Rhyodacite	UDPN 3-plg Plagioclase	CDCM-1 Basalt
La	47.1	3.59	14.9
Ce	87.3	5.46	33.8
Pr	10.6	0.54	4.96
Nd	42.1	1.82	21.1
Sm	7.52	0.25	5.13
Eu	2.26	1.64	2.01
Gd	7.35	0.22	6.08
Tb	1.01	0.021	0.98
Dy	5.56	0.11	5.64
Ho	1.04	0.016	1.18
Er	2.8	0.042	3.33
Tm	0.42	< 0.005	0.44
Yb	2.68	< 0.01	2.84
Lu	0.38	< 0.005	0.39

involve large-scale chemical diffusion between adjacent magma batches of different composition but similar temperature. Trace element exchange being more efficient in mixing environments than major element exchange, has been recorded for several mixed magma occurrences and net-veined complexes (e.g. O'Hara 1977; Gamble 1979; Cramer and Kwak 1988; Tindle 1991; Wiebe 1996; Poli et al. 1996) and is thought to be a function of higher diffusivities being associated with high-field-strength elements (Tindle 1991; Poli et al. 1996). To allow high diffusive fluxes of an element between contrasting magmas, thermal and density equilibrium have to be approached, however, before significant diffusion can occur (Huppert and Sparks 1980; Blake and Koyaguchi 1991; Koyaguchi and Blake 1991). This is probably best achieved through a semi-stable interface between rhyodacite and basalt in the magma chamber. There, the chemical exchange of species by molecular diffusion is overtaken by heat transfer and thermal equilibrium can be closely approached, although the major element character of the magma end-members is largely preserved, as seen in Rum type II inclusions (cf. Koyaguchi and Blake 1991).

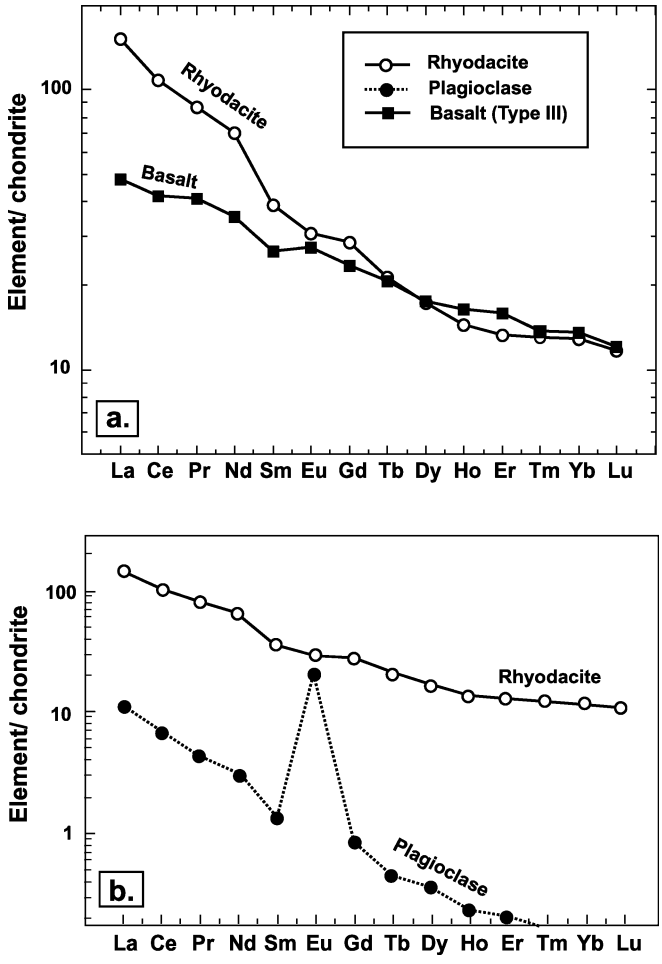

Fig. 8 **a** Chondrite-normalised REE plot of the rhyodacite and the basalt end-members and of **b** rhyolite and plagioclase separated from rhyodacite. See text for details

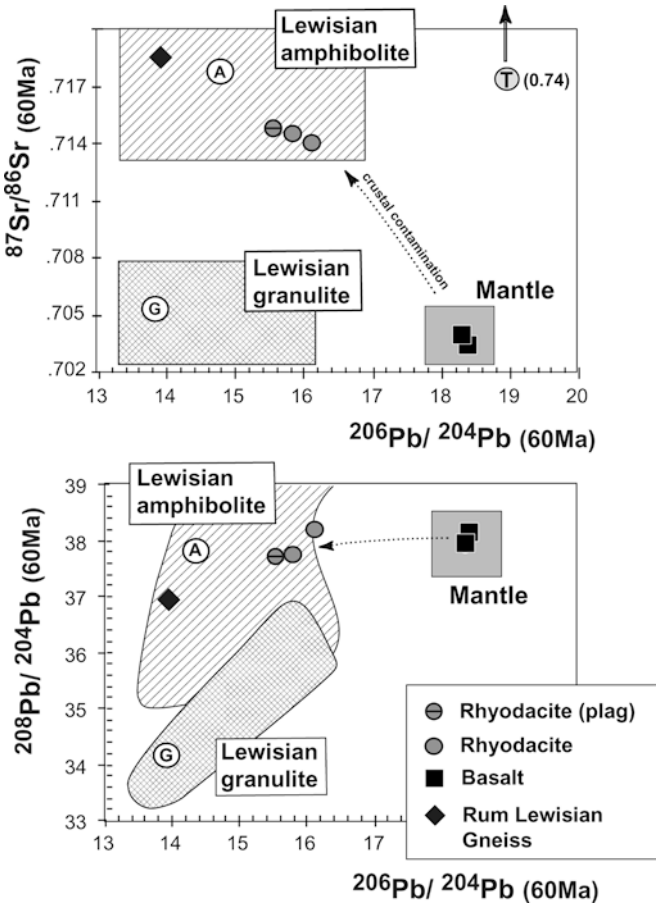

Fig. 9 **a** $^{87}Sr/^{86}Sr$ vs. $^{206}Pb/^{204}Pb$ and **b** $^{208}Pb/^{204}Pb$ vs. $^{206}Pb/^{204}Pb$ isotope ratio plots show the basalt and rhyodacite samples to be distinct in their isotope signature. The basalts plot in the sub-Hebridean mantle array, whereas the rhyodacites are strongly displaced towards average Lewisian amphibolite (*dotted lines*). *A* = Average Lewisian Amphibolite, *G* = Average Lewisian Granulite, *T* = Torridonian sandstone after Dickin 1981 and Thompson et al. 1986. Reference fields are compiled from Dickin 1981, Kerr et al. 1995, Geldmacher et al. 1998, 2001 and references therein)

A violent fountain replenishment, in turn, would favour hybridisation by e.g. bulk mixing along the fountains margins, as any kind of interface between the magma end-members would be highly unstable (cf. Campbell and Turner 1989; Koyaguchi and Blake 1991), thus being a less likely scenario for element diffusion between magma batches.

Three major mixing mechanisms are therefore distinguished for the Rum rhyodacites: (a) bulk mixing (hybridisation) by blending of two magmas, through the entrainment of one magma into another; (b) trace element diffusion across compositional interfaces of contrasting magma types along semi-stable interface(s) and (c) dispersion of liquid mafic magma by forced mingling

Table 4 Sr amd Pb isotopic ratios of Rum samples

Sample	Rock type	Location (NGRS)	$^{87}Sr/^{86}Sr_m$	Rb ppm	Sr ppm	$^{87}Sr/^{86}Sr$ (60 Ma)	$^{206}Pb/^{204}Pb$ (60 Ma)	$^{207}Pb/^{204}Pb$ (60 Ma)	$^{208}Pb/^{204}Pb$ (60 Ma)
CDCM-1-1	Basalt	387/984	0.703211(9)	35	300	0.702923	18.37	15.41	38.10
CDCM-1-2	Basalt	387/984	0.703236(8)	33	305	0.702969	18.32	15.42	37.96
STLH	Rhyodacite	387/981	0.715048(6)	89	237	0.714121	15.74	14.97	37.72
UDPN-3	Rhyodacite	385/986	0.714859(6)	92	169	0.713516	16.10	15.11	38.19
UDPN-plg	Plagioclase	358/986	0.714223(9)	1.5	264	0.714209	15.49	14.91	37.69
SR321B	Lew. gneiss	336/004	0.718691(7)	15	285	0.718560	13.95	14.56	36.96

Location of sampling site coordinates refer to the British National Grid Reference System (NGRS)
All lie within square NM (except for SR321B in NG). All errors are quoted at the 2 sigma level. Pb data from Geldmacher et al. (2001)

upon eruption, coupled with vesiculation and (explosive) disaggregation of mafic magma batches (Fig. 5).

Origin of the end-member magmas

The basaltic end-member of the rock suite displays elevated values of FeOt, TiO_2 and P_2O_5, an enriched signature on a chondrite-normalised REE variation diagram, and it plots in the mantle array in radiogenic isotope space. Much of this Fe–Ti–P-enriched basalt that entered the rhyodacite chamber appears to have been trapped beneath the felsic rhyodacite cap, because of its density, and interaction with the rhyodacite host magma followed in a common magma reservoir. The composition of this basaltic end-member closely resembles, for example the Fe–Ti–P-enriched 'Plateau Group' of the Mull Centre. Kerr et al. (1999) have argued that these plateau lavas originated from small degrees of melting of a dry garnet lherzolite, while the Central Mull tholeiites formed by larger degrees of partial melting of a spinel lherzolite. The Mull Plateau lavas also show a low degree of interaction with the crust (Thompson et al. 1986), unlike the Central Mull tholeiite magmas that are markedly contaminated and lack Fe–Ti–P enrichment (Thompson et al. 1986; Kerr et al. 1999). Given that Mull Plateau lavas and the early Rum basalts may be of different age (M. Pringle pers. com. and Troll unpublished data), it appears that early basaltic magmas in the Tertiary centres originated from low degrees of partial melting deep below the individual central volcanoes, rather than by a regionally supplied magma of homogeneous composition.

The origin of the rhyodacites is best reflected in their REE and isotopic composition. The rocks contain a substantial crustal component, indicating that the magma must have been emplaced in a shallow crustal storage reservoir considerably before intrusion of the inclusion-forming magma to allow for massive assimilation of Lewisian country-rock. The cross-cutting REE pattern of rhyodacite and co-existing basalt indicates distinct petrogenetic histories for the two magmas, as purely derivative liquids tend to have patterns parallel to their parental magma on such a plot (Bell 1983). The parental magma to the rhyodacite is no longer recognisable because of severe modification through fractionation and assimilation in the crustal storage reservoir, and through magma mixing with crustally uncontaminated mantle-derived basalt. This contrasts with certain other complexes of the British Tertiary Igneous Province in which the mafic and felsic rocks both show isotopic evidence of crustal interaction, consistent with continuous differentiation sequences such as 'assimilation during turbulent ascent' (Kerr et al. 1995) and 'assimilation and fractional crystallisation' (Geldmacher et al. 1998). In the Rum case, however, the data show that the basaltic and other mafic inclusions are not related to the rhyodacite through a differentiation series; rather they indicate that the mafic end-member derived from a distinct source

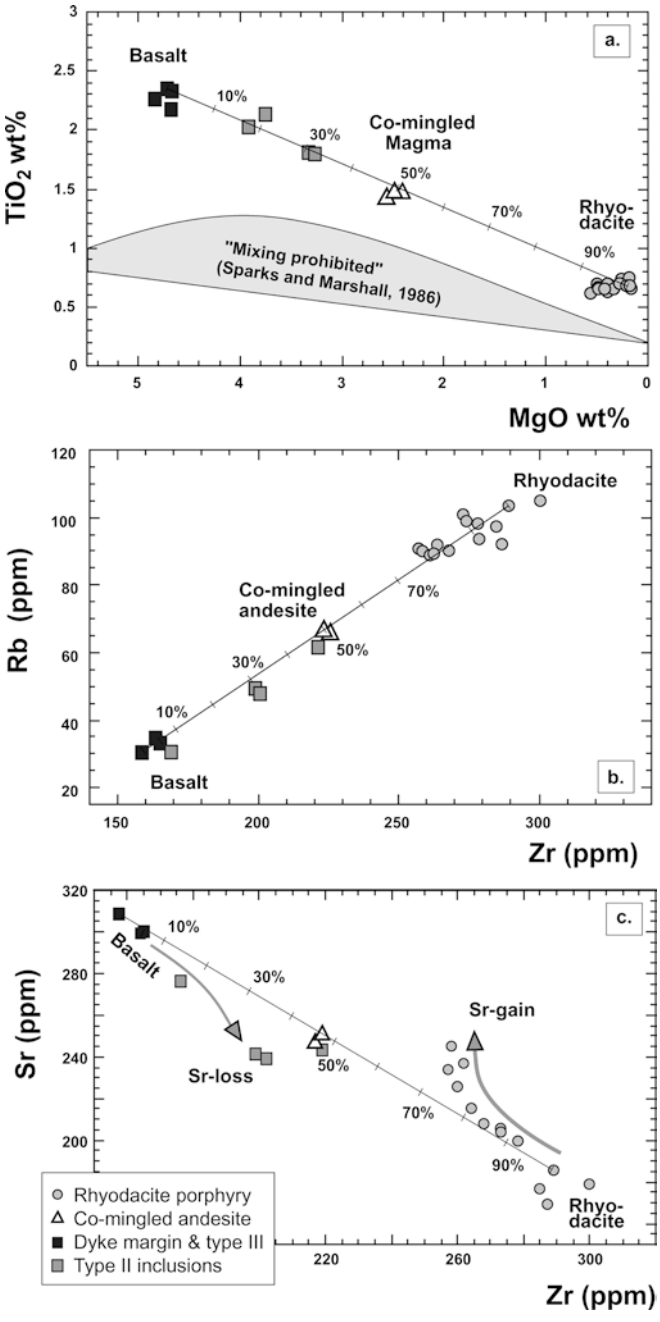

Fig. 10 **a** MgO vs TiO_2 variation shows the sample suite plots beyond the field of prohibited mixing. The most hybridised mafic inclusions are a mixture of 70% basalt and 30% rhyodacite. The co-mingled andesite samples, by contrast, represent a 50:50 mixture. The rhyodacite samples form a tight cluster, apparently unaffected by mixing. **b** Zr vs. Rb (ppm), in turn, shows the most hybridised mafic enclaves represent an almost 50:50 basalt - rhyodacite mixture in their incompatible trace element concentrations and that the rhyodacite is a mixture of up to 25% basalt derived trace elements for the most affected samples. Note the co-mingled andesite samples are a 50:50 mixture for major and for trace elements. **c** Zr vs. Sr variation indicates a relative gain of Sr by the rhyodacite, and a relative depletion of Sr in the mafic inclusions (see text for details)

and that the two magmas probably first met in the shallow rhyodacite magma chamber. Figure 11 shows a binary mixing curve (BM) between the local crust

(Lewisian) and the most mafic basalt, with the rhyodacite samples plotting directly on this curve. Also shown are two AFC model calculations (cf. DePaolo 1981) that simulate fractional crystallisation of basalt magma and simultaneous assimilation of Lewisian gneiss. The AFC curve to the right shows a moderate mass assimilation rate to fractional crystallisation rate ($r = 0.5$) and the left curve a relatively high rate of assimilation to crystal fractionation ($r = 0.8$). Neither of the AFC curves intersects with the rhyodacite samples, implying that binary mixing of two or more unrelated magmas was the pre-dominant process. This view that the two end-member magmas have distinct histories is consistent with a recent proposal by Eichelberger et al. (2000), suggesting that co-eruptive magmas are often not co-genetic, emphasising the importance of magma mixing in producing a diversity of magma compositions. An earlier mafic magma, however, must have been the driving force for the generation of the rhyodacite magma (cf. Thompson 1980), possibly represented in some of the earlier gabbros exposed in the Northern Marginal Zone (Emeleus 1997). The actual amount of crustal contribution to the rhyodacites is difficult to assess since country-rock melting was most likely a selective melting process as suggested by partial melting textures in Lewisian samples from Rum (see Emeleus 1997). Textures in these samples show that hydrous phases were melted preferentially, implying that contamination would be strongest for those elements that are concentrated in e.g. mica and amphibole. This observation is consistent with the more radiogenic Sr and Pb ratios in the rhyodacite's feldspar relative to the bulk rock, implying selective contamination with input of highly radiogenic components first (cf. Duffield and Ruiz 1998).

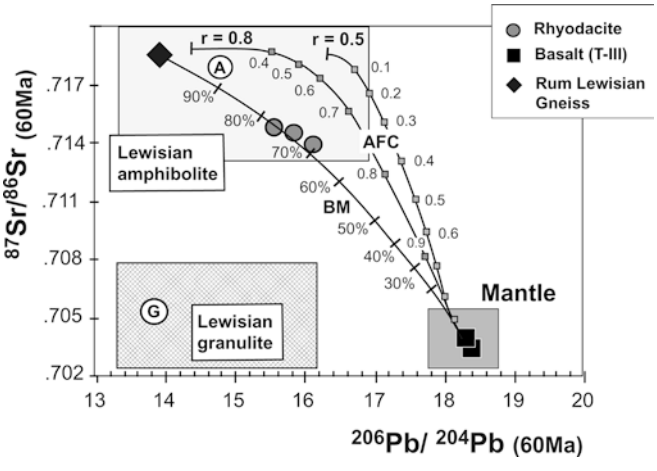

Fig. 11 $^{87}Sr/^{86}Sr$ vs. $^{206}Pb/^{204}Pb$ plot with superimposed binary mixing trajectory between the most mafic basalt sample and Lewisian country-rock (*BM*). Also shown are AFC curves with a moderate mass assimilation rate to fractional crystallisation rate ($r = 0.5$) and a high mass assimilation rate to fractional crystallisation rate ($r = 0.8$). Rhyodacite data plot on binary mixing trajectory and do not intersect either of the two AFC curves. Numbers on AFC curves indicate fraction of melt remaining. See text for details

Quantification, using binary mixing models, is therefore likely to overestimate the overall crustal input as radiogenic Sr would be preferentially concentrated in the hydrous minerals of the Lewisian country-rock. It is, however, safe to conclude that a substantial proportion of the rhyodacite magma was of crustal, rather than purely magmatic origin.

A model for the Rum rhyodacite–basalt association

The combined evidence from field observations, petrography, mineral zoning and geochemistry supports a model in which pre-eruptive mixing and hybridisation was permitted by temperature and compositional differences of the magmas, but was slow due to their contrasted density and viscosity. The basic magma that entered the chamber by fountaining (type III inclusions) accumulated largely at the chamber floor where it cooled and began to de-gas. Soon the upper part of the accumulated mafic magma equilibrated thermally with the lower temperature rhyodacite magma. During and following this stage there was blending of the two compositions plus exchange of specific trace elements between the two magmas (type II inclusions). Eruption was probably caused by replenishment with, and degassing of, the basic magma (Troll et al. 2000), as inferred from vesicular inclusions of both type II and type III. In this case the time between thermal equilibration and eruption was relatively short. This is consistent with the radiogenic isotope data that imply that the least-evolved type II basalt did not have sufficient residence time in the rhyodacite reservoir to take up the crustal isotope signature of the extensively contaminated rhyodacite and/or of the wall rock.

The evidence supports the following interpretation. A major pulse of primitive, mantle-derived, high Fe–Ti–P basalt magma replenished the rhyodacite storage chamber. Initial chilling of the arriving basalt produced type III inclusions by (a) break-up of the replenishing fountain and perhaps (b) buoyant rise of vesiculated basalt blobs subsequently distributed throughout the rhyodacite by convection. However, the major part of the basalt accumulated and/or spread across the chamber floor and formed a semi-stable basalt layer in the chamber (Fig. 12A). From the linear relationship of FeOt, MgO and TiO_2 a density stratification of the magmas from basalt at the bottom through hybrid andesite to rhyodacite is inferred (Fig. 12B). The well-blended andesitic magma layer probably resulted from entrainment of rhyodacite in basalt and element diffusion across compositional interfaces of blobs and inclusions and/or along a more or less stable horizontal interface between the two magma layers. Further replenishments could have entered the chamber after mixing was initiated and disrupted the chamber stratification, enhancing physical mingling and chemical mixing and causing successive dis-equilibrium reactions and textures such as complex multiple zoning in the

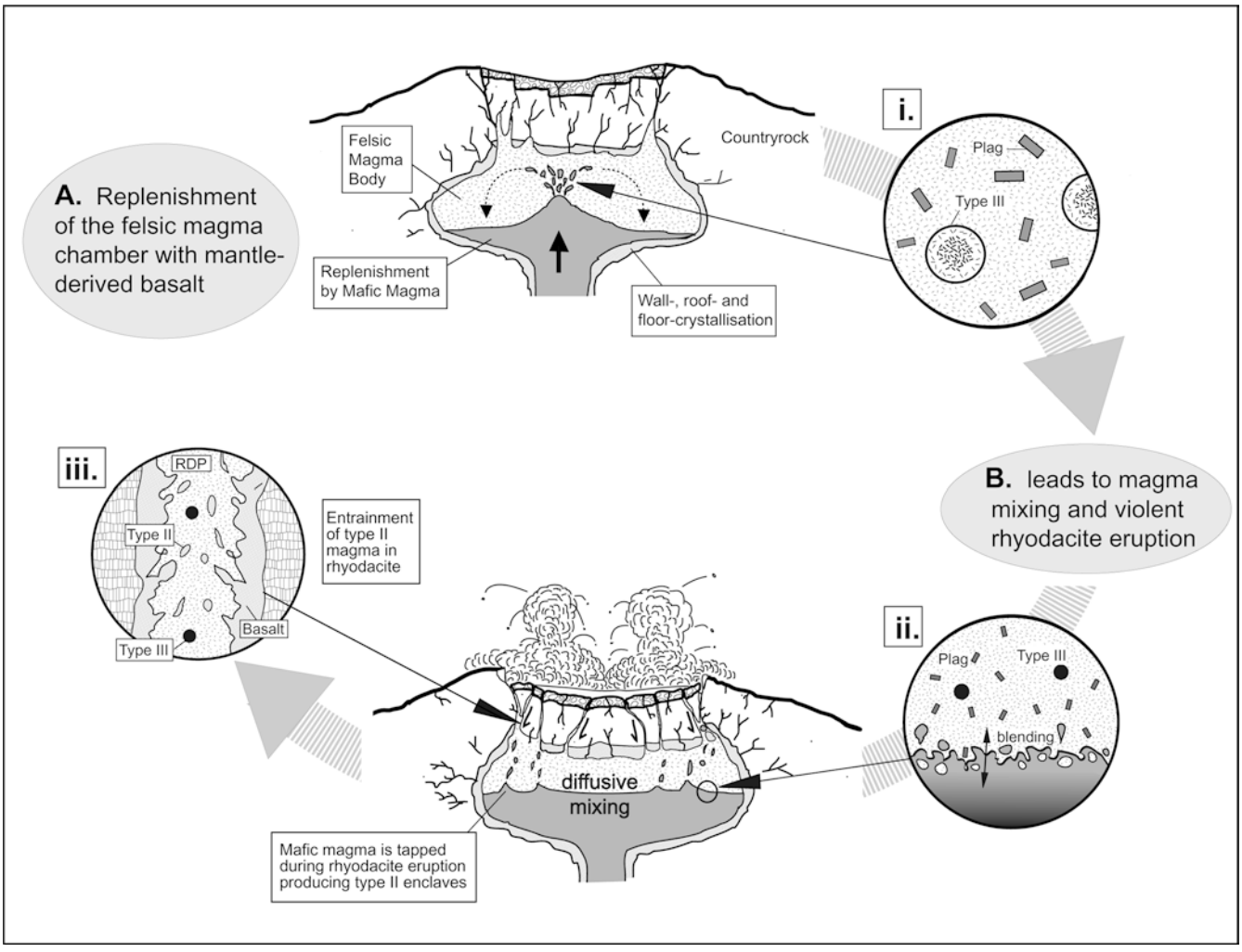

Fig. 12A,B Interpretation of magma chamber evolution and eruption processes. **A** Reconstruction of pre-eruptive internal magma chamber structure, where basaltic magma is injected into the rhyodacite reservoir. (i) Chilled mafic inclusions (type III) form by disaggregation of the injected fountain and chilling against the cooler rhyodacite host. This produces a characteristic increase of crystal size in the type III inclusions. **B** The bulk of the mafic magma forms a denser bottom layer in the chamber separated from the lighter rhyodacite through a semi-stable interface. (ii) Blending (bulk-mixing) and element diffusion (indicated by the arrow) act along this/these interface(s) producing a hybrid but trace element-enriched andesite magma (type II inclusions). (iii) On eruption the hybrid andesite and the rhyodacite magmas experience physical mingling in the conduit, coupled with violent vesiculation and further disintegration of the mafic magma blobs

rhyodacite's phenocrysts. The replenishments and continuing degassing of the mafic magma are likely to have caused overpressurisation of the magma chamber and its contents and triggered the violent ash-flow eruption (cf. the models of Sparks et al. 1977; Eichelberger 1980; Folch and Marti 1998). Dispersion of liquid mafic magma by forced mingling upon eruption then followed during transport of magma from the magma chamber to the surface (cf. Freundt and Tait 1986), as observed in the composite dykes and plug of the Northern Marginal Zone. There, further vesiculation on decompression increased the (explosive) disaggregation of mafic magma batches.

Conclusion

The rhyodacites of the Northern Marginal Zone represent intra-caldera ash-flow sheets that are connected to their feeder dykes. The rhyodacites record evidence of violent magma mingling in the eruption conduit as well as pre-eruptive diffusive mixing in the magma chamber. The magma chamber was partially evacuated while the process of magma hybridisation was underway and erupted two distinct end-member magmas (basalt and rhyodacite), together with various mixed mafic-intermediate compositions. Mixing of magmas was achieved through (a) hybridisation by blending of two magmas, (b) trace element diffusion across compositional interfaces, and (c) dispersion of liquid mafic magma by forced mingling upon eruption. The combined evidence points towards magma mixing in a multiple-replenished chamber, where degassing of incoming mafic magma triggered the explosive ash-flow eruptions. The mafic magma was not related to the rhyodacite. Instead, the

two magmas are derived from distinct sources, being thus co-eruptive but not co-genetic.

Acknowledgements We are grateful to the Scottish Natural Heritage for permission to work on the island and to M. Hendry for field support. K. Atkinson drafted an earlier version of the map and U. Thurow helped with some of the other figures. Thanks are also due to A. Mackie (sample preparation), A. Calder and D. Rau (XRF), D. Herd (EMP), and particularly to F. Hauff for access to the Geomar TIMS facilities. B. Wenskowski, S. Duggen, M. Abratis, and S. Vetter are thanked for assistance and good company during data acquisition at GEOMAR. Discussion with J. Gamble, C. Stillman, W.E. Stephens and J. Reavey is greatly appreciated and B. Upton and A. Kerr are thanked for stimulating journal reviews. CHD and VRT received financial support from the Welsh Bequest of the University of St Andrews.

References

Almond DC (1971) Ignimbrite vents in the Sabaloka cauldron, Sudan. Geol Mag 108:159–176

Bacon CR (1986) Magmatic inclusions in silicic and intermediate volcanic rocks. J Geophys Res 91:6091–6112

Bailey EB (1945) Tertiary igneous tectonics of Rhum (Inner Hebrides). J Geol Soc Lond 100:165–188

Bell BR (1983) Significance of ferrodioritic liquids in magma mixing processes. Nature 306: 323–327

Bell BR, Emeleus CH (1988) A review of silicic pyroclastic rocks of the British Tertiary Volcanic Province. In: Morton A, Parson L (eds) Early Tertiary volcanism and the Opening of the NE-Atlantic. Geol Soc Spec Pub 39:365–379

Blake DH, Elwell RWD, Gibson IL, Skelhorn RR, Walker GPL (1965) Some relationships resulting from the intimate association of acid and basic magmas. J Geol Soc Lond 121:31–49

Blake S, Koyaguchi T (1991) Insights on the magma mixing model from volcanic rocks. In: Didier J, Barbarin B (eds) Enclaves in granite petrology. Elsevier, Amsterdam, pp 403–413

Campbell IH, Turner JS (1989) Fountaining in magma chambers. J Petrol 30:885–923

Civetta L, Dàntonio M, Orsi G, Tilton G (1998) The Geochemistry of volcanic rocks from Pantelleria Island, Sicily Channel: petrogenesis and characteristics of the mantle source region. J Petrol 39:1453–1491

Coombs ML, Eichelberger JC, Rutherford MJ (2002) Experimental and textural constraints on mafic enclave formation in volcanic rocks. J Volcanol Geotherm Res 119:125–144

Cramer JJ, Kwak TAP (1988). A geochemical study of zoned inclusions in granitic rocks. Amer J Sci 288:827–871

DePaolo DJ (1981) Trace element and isotopic effects of combined wall-rock assimilation and fractional crystallisation. Earth Planet Sci Lett 53:189–202

Dickin AP (1981) Isotope geochemistry of Tertiary igneous rocks from the Isle of Skye, N.W. Scotland. J Petrol 22:155–189

Donaldson CH, Troll VR, Emeleus CH (2001) Felsites and breccias in the Northern Marginal Zone of the Rum Igneous Complex: changing views ca. 1900–2000. Proc Yorksh Geol Soc 53:167–175

Duffield WA, Ruiz J (1998) A model that helps explain Sr-isotope disequilibrium between feldspar phenocrysts and melt in large silicic magma systems. J Volcanol Geotherm Res 87:7–13

Dunham AC (1965) The nature and origin of the groundmass textures in felsites and granophyres from Rhum, Inverness-shire. Geol Mag 102:8–23

Dunham AC (1968) The felsites, granophyre, explosion breccias and tuffisites of the north-eastern margin of the Tertiary igneous complex of Rhum Inverness-shire. J Geol Soc Lond 123:327–352

Eichelberger JC (1980) Vesiculation of basic magma during replenishment of silicic magma reservoirs. Nature 288:446–450

Eichelberger JC, Chertkoff DG, Dreher ST, Nye CJ (2000) Magmas in collision: rethinking chemical zonation in silicic magmas. Geology 28:603–606

Ellam RM, Stuart FM (2000). The sub-lithospheric source of North Atlantic basalt: evidence for, and significance of, a common end-member. J Petrol 41:919–932

Elwell RW, Brück PM, O'Connor PJ (1974) Granophyre net-veining in the dolerites of Slieve Gullion. Proc Roy Irish Acad 74:439–454

Emeleus CH, Dunham AC, Thompson RN (1971) Iron-rich pigeonites from acid rocks in the Tertiary igneous province of Scotland. Amer Mineral 56:940–951

Emeleus CH (1997) Geology of Rum and the adjacent islands. Memoir of the British Geological Survey, Sheet 60 (Scotland)

Folch A, Marti J (1998) The generation of overpressure in felsic magma chambers by replenishment. Earth Planet Sci Lett 163:301–314

Freundt A, Tait SR (1986) The entrainment of high viscosity magma into low viscosity magma in eruption conduits. Bull Volcanol 48:325–339

Freundt A, Schmincke H-U (1995) Petrogenesis of rhyolite-trachyte-basalt composite ignimbrite P1, Gran Canaria, Canary Island. J Geophys Res 100:455–474

Gamble J (1979) Some relationships between coexisting granitic and basaltic magmas and the genesis of hybrid rocks in the Tertiary central complex of Slieve Gullion, northeast Ireland. J Volcanol Geotherm Res 5:297–316

Geikie A (1888) The history of volcanic action during the Tertiary period in the British Isles. Trans Roy Soc Edinburgh 35:21–184

Geldmacher J, Haase KM, Devey CW, Garbe-Schönberg CD (1998) The petrogenesis of the Tertiary cone-sheets in Ardnamurchan, NW-Scotland: petrological and geochemical constraints on crustal contamination and partial melting. Contrib Mineral Petrol 131:196–209

Geldmacher J, Troll VR, Emeleus CH, Donaldson CH (2002) Pb-isotope evidence for contrasting crustal contamination of primitive to evolved magmas from Ardnamurchan and Rum: implications for the structure of the underlying crust. Scott J Geol 38:55–61

Hamilton MA, Pearson DG, Thompson RN, Kelley SP, Emeleus CH (1998) Rapid eruption of Skye lavas inferred from precise U-Pb and Ar-Ar dating of the Rum and Cuillin plutonic complexes. Nature 394:260–263

Harker A (1904) The Tertiary igneous rocks of Skye. Memoir of the Geological Survey, Scotland, Sheet 418

Harker A (1908) The Geology of the Small Isles of Inverness-shire. Memoir of the Geological Survey, Scotland, Sheet 60

Hoernle K, Tilton G, Schmincke H-U (1991) Sr-Nd-Pb isotopic evolution of Gran Canaria: evidence for shallow enriched mantle beneath the Canary Islands. Earth Planet Sci Lett 106, 44–63

Hughes CJ (1960) The Southern Mountains igneous complex, Isle of Rhum. J Geol Soc Lond 116:111–138

Huppert HE, Turner JS (1981) A laboratory model of a replenished magma chamber. Earth Planet Sci Lett 54:144–152

Huppert HE, Sparks RSJ (1980) The fluid dynamics of a basaltic magma chamber replenishment by influx of hot, dense ultrabasic magma. Contrib Mineral Petrol 75:279–289

Judd JW (1874) The secondary rocks of Scotland; On the ancient volcanoes of the highlands and the relations of their products to the Mesozoic strata. J Geol Soc London 30:220–301

Kerr AC, Kempton PD, Thompson RN (1995) Crustal assimilation during turbulent magma ascent (ATA); new isotopic evidence from the Mull Tertiary lava succession, N.W. Scotland. Contrib Mineral Petrol 119:142–154

Kerr AC, Kent RW, Thomson BA, Seedhouse JK, Donaldson CH (1999) Geochemical evolution of the Tertiary Mull volcano, Western Scotland. J Petrol 40:873–908

Koyaguchi T, Blake S (1991) Origin of mafic enclaves: Constraints on the magma mixing model from fluid dynamic experiments. In: Didier J and Barbarin B (eds) Enclaves in Granite petrology. Elsevier, Amsterdam, pp 415–429

Lipman PW (1976) Caldera-collapse breccias in the western San Juan Mountains, Colorado. Geol Soc Amer Bull 87:1397–1410

Lofgren GE (1980) Experimental studies on the dynamic crystallisation of silicate melts. In: Hargraves RB (ed) Physics of magmatic processes. Princeton University Press, pp 487–554

Marshall LA, Sparks RSJ (1984) Origin of some mixed-magma and net-veined ring intrusions. J Geol Soc Lond 141:171–182

Nixon GT, Pearce TH (1987) Laser-interferometry study of oscillatory zoning in plagioclase: the record of magma mixing and phenocryst recycling in calc-alkaline magma chambers, Iztaccihuatl volcano, Mexico. Amer Mineral 72:1144–1162

O'Hara MJ (1977) Geochemical evolution during fractional crystallisation of a periodically refilled magma chamber. Nature 266:503–507

Pearce TH, Kolisnik AM (1990) Observations of plagioclase zoning using interference imaging. Earth Sci Rev 29:9–26

Platevoet B, Bonin B (1991) Enclaves and mafic–felsic associations in the Permian alkaline province of Corsica, France: physical and chemical interactions between coeval magmas. In Didier J and Barbarin B (eds) Enclaves in granite petrology. Elsevier, Amsterdam, pp 191–204

Poli G, Tommasini S, Halliday A (1996) Trace element and isotopic exchange during acid-basic magma interaction processes. Trans Roy Soc Edinburgh 87:225–232

Sparks RSJ (1988) Petrology and geochemistry of the Loch Ba ring dyke, Mull (N.W. Scotland): an example of the extreme differentiation of tholeiitic magmas. Contrib Mineral Petrol 100:446–461

Sparks RSJ, Marshall LA (1986) Thermal and mechanical constraints on mixing between mafic and silicic magmas. J Volcanol Geotherm Res 29:99–124

Sparks RSJ, Sigurdsson H, Wilson L (1977) Magma mixing: A mechanism for triggering acid explosive eruptions. Nature 267:315–318

Stamatelopoulou-Seymour K, Vlassopoulos D, Pearce T, Rice C (1990) The record of magma chamber processes in plagioclase phenocrysts at the Thera Volcano, Aegean Volcanic Arc, Greece. Contrib Mineral Petrol 104:73–84

Tepley FJ, Davidson JP, Clynne MA (1999) Magmatic interactions as recorded in plagioclase phenocrysts of Chaos Crags, Lassen volcanic center, California. J Petrol 40:787–806

Tindle AG (1991) Trace element behaviour in microgranular enclaves from granitic rocks. In: Didier J and Barbarin B (eds) Enclaves in granite petrology. Elsevier, Amsterdam, pp 313–330

Thompson RN (1980) Askja 1875, Skye 56 Ma: basalt-triggered, plinian, mixed–magma eruptions during the emplacement of the Western Redhills granites, Isle of Skye, Scotland. Geol Rundsch 69:245–262

Thompson RN, Morrison MA, Dickin AP, Gibson IL, Harmon RS (1986) Two contrasting styles of interaction between basic magmas and continental crust in the British Tertiary Volcanic Province. J Geophys Res 91:5985–5997

Troll VR, Emeleus CH, Donaldson CH (2000) Caldera formation in the Rum central igneous complex, Scotland. Bull Volcanol 62:301–317

Troll VR, Schmincke H-U (2002) Alkali-feldspar in compositionally zoned peralkaline rhyolite/trachyte ignimbrite 'A', Gran Canaria: implications for magma mixing and crustal recycling. J Petrol 43:243–270

van Wagoner NA, Leybourne MI, Pearce TH, Timms CE (1995) Comparison of petrogenetic processes between the West Valley segment of Juan de Fuca Ridge and the adjacent Heck Chain of seamounts: Detailed Electron microprobe study and Normarski interference imaging of plagioclase. Can Mineral 33:569–583

Walker GPL (1984) Downsag calderas, ring faults, caldera sizes and incremental growth. J Geophys Res 89:8407–8416

Walker GPL, Skelhorn RR (1966) Some associations of acid and basic igneous rocks. Earth Sci Rev 2:9–109

Wiebe RA, Frey H, Hawkins DP (2001) Basaltic pillow mounts in the Vinalhaven intrusion, Maine. J Volcanol Geotherm Res 107:171–184

Wiebe RA (1996) Mafic-silicic layered intrusions: the role of basaltic injections on magmatic processes and the evolution of silicic magma chambers. Trans Roy Soc Edinburgh 87:233–242

Williams PJ (1985) Pyroclastic rocks of the Cnapan Breaca felsite, Rhum. Geol Mag 122:447–450